Fission modes of mercury isotopes

M. Warda,[1] A. Staszczak,[1,2,3] and W. Nazarewicz[2,3,4]
[1]*Institute of Physics, Maria Curie-Skłodowska University, pl. M. Curie-Skłodowskiej 1, 20-031 Lublin, Poland*
[2]*Department of Physics and Astronomy, University of Tennessee, Knoxville, Tennessee 37996, USA*
[3]*Physics Division, Oak Ridge National Laboratory, Oak Ridge, Tennessee 37831, USA*
[4]*Institute of Theoretical Physics, University of Warsaw, ul. Hoża 69, PL-00-681 Warsaw, Poland*
(Received 24 May 2012; published 7 August 2012)

Background: Recent experiments on β-delayed fission in the mercury-lead region and the discovery of asymmetric fission in ^{180}Hg [A. N. Andreyev *et al.*, Phys. Rev. Lett. **105**, 252502 (2010)] have stimulated theoretical interest in the mechanism of fission in heavy nuclei.
Purpose: We study fission modes and fusion valleys in ^{180}Hg and ^{198}Hg to reveal the role of shell effects in the prescission region and explain the experimentally observed fragment mass asymmetry and its variation with A.
Methods: We use the self-consistent nuclear density functional theory employing Skyrme and Gogny energy density functionals.
Results: The potential energy surfaces in multidimensional space of collective coordinates, including elongation, triaxiality, reflection-asymmetry, and necking, are calculated for ^{180}Hg and ^{198}Hg. The asymmetric fission valleys—well separated from fusion valleys associated with nearly spherical fragments—are found in both cases. The density distributions at scission configurations are studied and related to the experimentally observed mass splits.
Conclusions: The energy density functionals SkM* and D1S give a very consistent description of the fission process in ^{180}Hg and ^{198}Hg. We predict a transition from asymmetric fission in ^{180}Hg toward a more symmetric distribution of fission fragments in ^{198}Hg. For ^{180}Hg, both models yield ^{100}Ru/^{80}Kr as the most probable split. For ^{198}Hg, the most likely split is ^{108}Ru/^{90}Kr in HFB-D1S and ^{110}Ru/^{88}Kr in HFB-SkM*.

DOI: 10.1103/PhysRevC.86.024601 PACS number(s): 21.60.Jz, 24.75.+i, 27.70.+q, 27.80.+w

I. INTRODUCTION

The fission phenomenon is a magnificent example of a quantal large-amplitude collective motion during which the nucleus evolves in a multidimensional space representing shapes with different geometries, often tunneling through a classically forbidden region [1]. Understanding the fission process is crucial for many areas of science and technology. For instance, fission governs the existence of many transuranium elements, including the predicted long-lived super-heavy species. In nuclear astrophysics, fission influences the formation of heavy elements in a very high neutron density environment. Fission applications are numerous. For instance, improved understanding of the fission process will enable scientists to enhance the safety and reliability of nuclear reactors. While in the past the design, construction, and operation of reactors were supported through empirical trials, the new phase in nuclear energy production is expected to rely heavily on advanced modeling and simulation capabilities utilizing massively parallel leadership-class computers.

A comprehensive explanation of nuclear fission rooted in interactions between nucleons still eludes us, although self-consistent approaches based on the nuclear density functional theory (DFT) have recently demonstrated that a microscopic description has a potential for both qualitative and quantitative description of fission data [2–7]. A starting point in the adiabatic approach to fission is the capability to compute accurate multidimensional potential energy surfaces (PES), and use them to predict observables such as fission half-lives and fragment mass distributions.

This work has been stimulated by recent experiments on β-delayed fission in the mercury-lead region [8] and the discovery of asymmetric fission of the nucleus ^{180}Hg. Such an outcome has not been initially anticipated, as the symmetric fission channel involving two semimagic ^{90}Zr fragments was believed to dominate the process. It has been generally expected that the asymmetric fission is not important below ^{227}Th [9], in particular in pre-actinide nuclei with high-lying saddle-point configurations that depend weakly on shell effects [10]. Moreover, the data on mass distributions of fragments in the low-energy fission of nuclei with $187 \leqslant A \leqslant 213$ have demonstrated the strong presence of the symmetric fission mode [11]. In particular, the nucleus ^{198}Hg has been observed to exhibit a fairly broad mass distribution [11,12].

The explanation of the asymmetric fission around ^{180}Hg has been offered by the macroscopic-microscopic model [8,13] and its extension [14] in terms of an asymmetric fission pathway that is separated by a potential-energy ridge from the symmetric $^{90}\mathrm{Zr} + {}^{90}\mathrm{Zr}$ fusion valley. These results have emphasized the importance of shell effects between fission saddle and scission in pre-actinide nuclei (see also Ref. [15]). In this work, we extend the theoretical analysis of Ref. [8] using the self-consistent nuclear DFT. We explain the transition from the asymmetric fission in ^{180}Hg [8] to a more symmetric situation in ^{198}Hg [11] in terms of shell effects. We compare the fission pathways in both nuclei and discuss the interplay between fission and fusion valleys. Finally, by studying density distributions of fragments, we demonstrate that scission configurations of ^{180}Hg and ^{198}Hg can be understood in terms of molecular structures.

 ©2012 American Physical Society

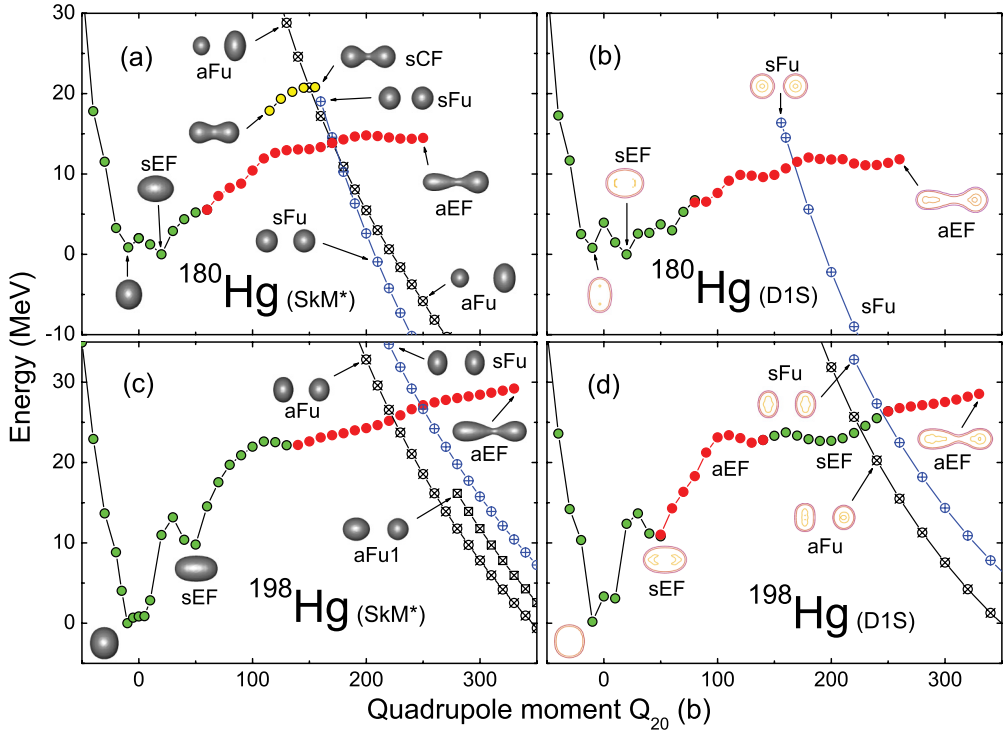

FIG. 1. (Color online) Fission pathways for ^{180}Hg (top) and ^{198}Hg (bottom) as functions of the driving quadrupole moment, Q_{20} calculated with HFB-SkM* (left) and HFB-D1S (right). Competing fission and fusion valleys are indicated, together with the associate shapes. Since the sEF configuration sometimes corresponds to a ridge (rather than a valley), the corresponding curves do not continue in such cases. See text for details.

II. MODEL

The Skyrme-HFB calculations were carried out using the framework previously discussed in Refs. [4,16,17] based on the symmetry unrestricted DFT solver HFODD [18] capable of breaking all self-consistent symmetries of nuclear mean fields on the way to fission. To solve a constrained nonlinear HFB problem precisely, we employed the augmented Lagrangian method [16]. The nuclear energy density functional was approximated by the SkM* functional [19] in the particle-hole channel and the density-dependent mixed pairing interaction [20] in the particle-particle channel. To truncate the quasiparticle space of HFB, we adopted the quasiparticle-cut-off value of 60 MeV in the equivalent energy spectrum [21]. The pairing strengths were adjusted to reproduce the neutron and proton pairing gaps in ^{252}Fm [4]; the resulting values are $V_{n0} = -268.9$ MeV fm^3 and $V_{p0} = -332.5$ MeV fm^3. The stretched harmonic oscillator (HO) basis of HFODD was composed of states having not more than $N_0 = 26$ quanta in either of the Cartesian directions and not more than 1140 states in total.

Our Gogny calculations follow the framework described in Refs. [2,22] based on the axial Gogny-HFB solver [23] and D1S parameter set [24]. We used the stretched HO basis with $N_z = 22$ HO shells along the symmetry axis and $N_\perp = 15$ shells in the perpendicular direction. The oscillator length was adjusted at every calculation point.

To find the optimum trajectories in a multidimensional collective space, we constrain the nuclear collective coordinates associated with the multipole moments $Q_{\lambda\mu}$, by which we explore the main degrees of freedom related to elongation ($\lambda\mu = 20$) and reflection-asymmetry ($\lambda\mu = 30$). In our symmetry unrestricted Skyrme-HFB calculations, we also

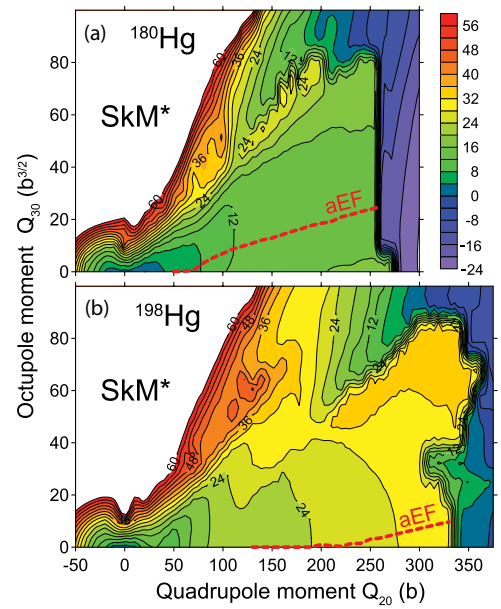

FIG. 2. (Color online) PES for ^{180}Hg (top) and ^{198}Hg (bottom) in the plane of collective coordinates Q_{20}–Q_{30} in HFB-SkM*. The aEF fission pathway corresponding to asymmetric elongated fragments is marked. The difference between contour lines is 4 MeV. The effects due to triaxiality, known to impact inner fission barriers in the actinides, are negligible here.

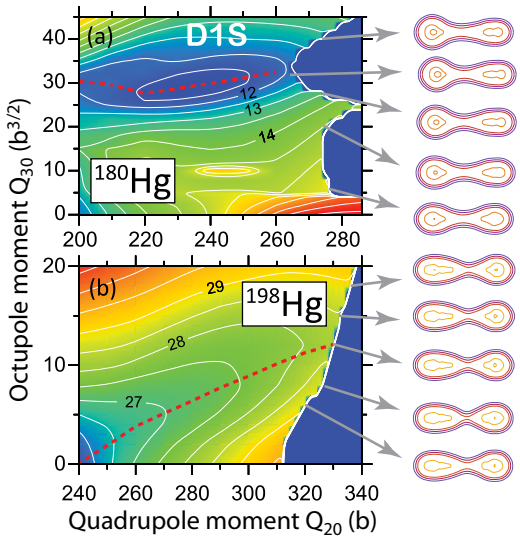

FIG. 3. (Color online) PES in HFB-D1S for ^{180}Hg (top) and ^{198}Hg (bottom) in the (Q_{20}, Q_{30}) plane in the prescission region of aEF valley. The symmetric limit corresponds to $Q_{30} = 0$. The aEF valley is marked by a dashed line. Density profiles for various prescission configurations are indicated. The difference between contour lines is 0.5 MeV. Note different Q_{30} scales in ^{180}Hg and ^{198}Hg plots.

explore the effects of triaxiality ($\lambda\mu = 22$) and necking ($\lambda\mu = 40$). In our axial Gogny calculations, the scission configurations were studied by means of the neck coordinate Q_N defined through the Gaussian-type operator $\hat{Q}_N = \exp[-(z - z_0)^2/a^2]$ with $a = 0.1$ fm and z_0 chosen to describe the neck region (e.g., $z_0 = 0.5$ fm in ^{180}Hg). Q_N describes the number of nucleons in a thin layer of thickness a perpendicular to the symmetry axis placed at $z = z_0$. Large values of Q_N describe shapes with a thick neck. By decreasing Q_N, one can approach the scission line. To obtain a PES, constrained HFB equations are solved to minimize the total energy of the system at each point in the collective space. As demonstrated earlier [4,5], exploring many collective coordinates makes it possible to identify saddle points [25] as the competing fission pathways are usually well separated when studied in more than one dimension.

III. COMPETING FISSION MODES

Figure 1 shows the calculated fission pathways in ^{180}Hg and ^{198}Hg. Both models predict a fairly similar pattern. The reflection symmetric fission path associated with elongated fragments (sEF) can be found for small deformations. The reflection-asymmetric path, corresponding to elongated fission fragments (aEF) of different masses and shapes, is branching away from the symmetric valley below $Q_{20} = 100$ b, and it passes through the mass asymmetric scission point (see Fig. 2 for a better view of aEF in the Q_{20}–Q_{30} plane).

In ^{180}Hg, at large elongations, the aEF path is strongly favored over reflection-symmetric configurations ($Q_{30} = 0$) associated with elongated fragments (sEF) and the symmetric compact fragment valley sCF—marked in Fig. 1(a). The fusion valleys, both symmetric (sFu) and asymmetric (aFu), appear very low in energy above $Q_{20} \approx 200$ b; they are associated with postscission configurations in which the two fragments

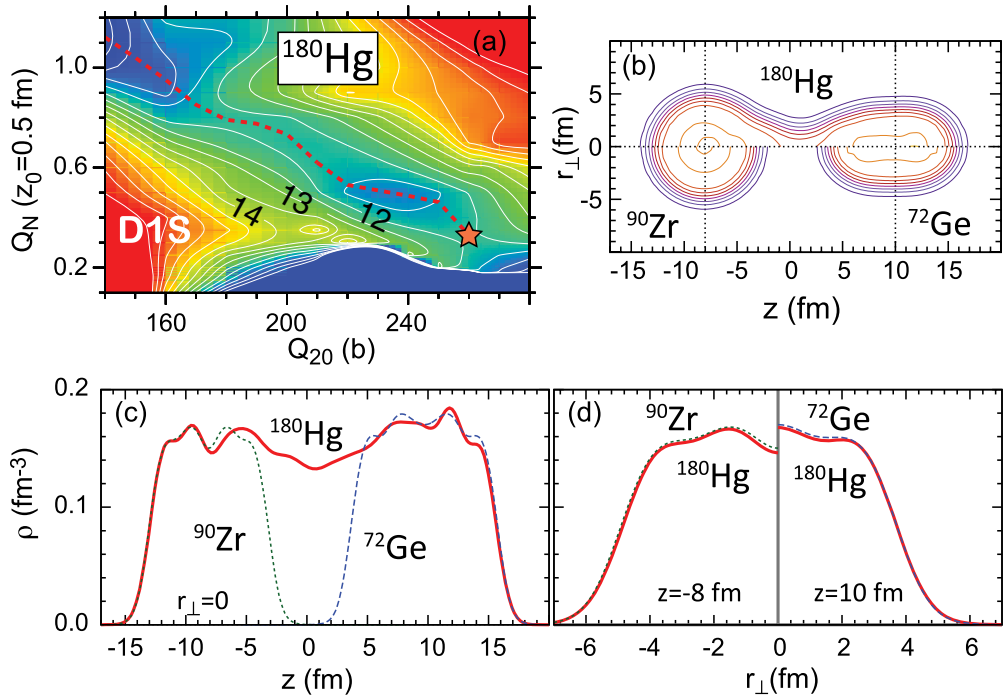

FIG. 4. (Color online) (a) PES of ^{180}Hg in the (Q_{20}, Q_N) plane computed in HFB-D1S in the scission region of aEF. (b) Density distribution in ^{180}Hg close to scission at $Q_{20} = 260$ b, $Q_N = 0.3$, and $Q_{30} = 33.8$ b$^{3/2}$ [marked by a star in panel (a)] compared to density distributions of ^{90}Zr (in its spherical ground state) and ^{72}Ge (in the excited deformed configuration with $Q_{20} = 8$ b). The density profiles for $r_\perp = 0$ (c), and for $z = -8$ fm and $z = 10$ fm (d) along the cuts marked by dotted lines in panel (b).

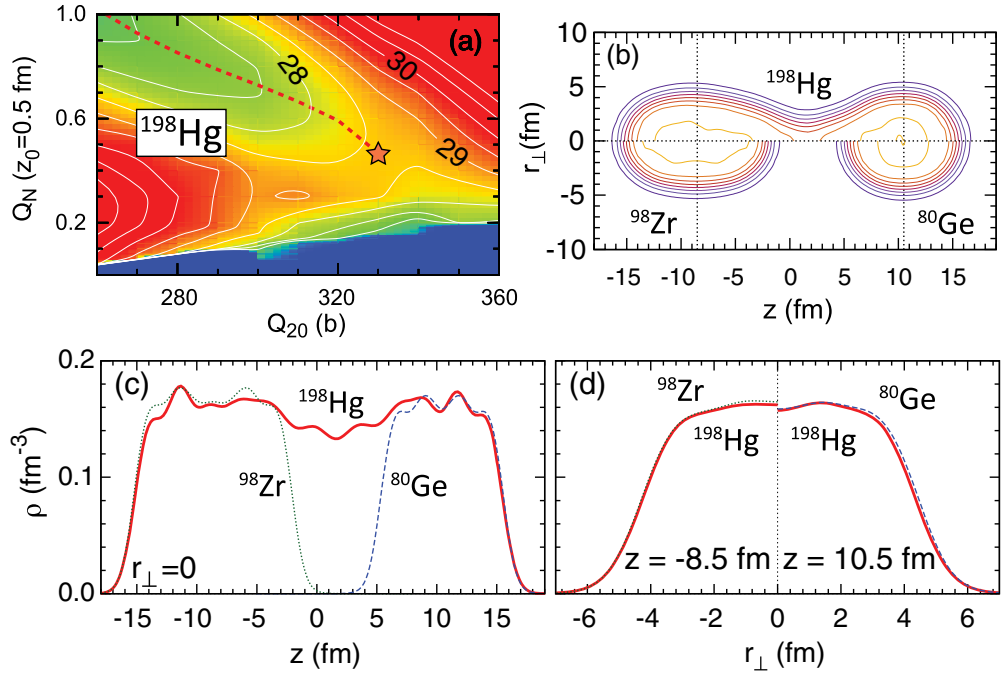

FIG. 5. (Color online) Similar as described in the legend of Fig. 4 but for ^{198}Hg. Density distributions of ^{198}Hg in (b)–(d) correspond to $Q_{20} = 330$ b, $Q_N = 0.33$, and $Q_{30} = 12.1$ b$^{3/2}$. They are compared to those of ^{98}Zr (in the excited deformed configuration with $Q_{20} = 12$ b) and ^{80}Ge (in its prolate ground state with $Q_{20} = 2.4$ b).

are well separated. Since the fission process is adiabatic, sFu and aFu are not expected to couple to aEF, which has a very distinct compound configuration exhibiting a pronounced neck even at $Q_{20} \approx 250$ b.

The situation in ^{198}Hg is qualitatively similar but the mass asymmetry along aEF is significantly reduced, and the energy difference between aEF and sEF (corresponding to $Q_{30} = 0$ in Fig. 2) is small, i.e., the PES is soft in the octupole direction as one approaches the saddle. In HFB-D1S calculations of Fig. 1(d), the energy balance between these two configurations is so fragile that a local transition from aEF to sEF, and back, is predicted at large deformations. This topography is consistent with a broad mass distribution of fission fragments observed in this nucleus. It is interesting to see that the magic structure of ^{90}Zr manifests itself in a very low energy of sFu in ^{180}Hg (^{90}Zr + ^{90}Zr) in both models. The asymmetric fusion valleys aFu become more favored in ^{198}Hg.

IV. PRESCISSION CONFIGURATIONS

The properties of fission fragments are governed by the nature of scission configurations at which a nucleus splits [26]. The scission point is not precisely defined in the models yielding leptodermous densities. We assume that a scission configuration corresponds to a well-defined thin neck, and for greater elongations the neck decreases and the binding energy rapidly drops due to the Coulomb repulsion between the fragments. For the detailed analysis, the hypersurface of scission points in the collective space has to be computed [6]. To get more insight into the mass distributions of fissioning Hg nuclei, in Fig. 3 we show the topography of PES for ^{180}Hg and ^{198}Hg obtained in HFB-D1S for prescission configurations around the aEF valley. It is gratifying to see that the predictions of HFB-D1S and HFB-SkM* (shown in Fig. 2) are similar. Namely, in both cases the aEF valley is separated by a ridge from the symmetric $Q_{30} = 0$ line (sEF) for ^{180}Hg, while for ^{198}Hg the prescission surface is fairly soft in the Q_{30} direction, and the aEF pathway corresponds to much smaller mass asymmetries.

The profiles of the density distribution for various configurations are also plotted in Fig. 3. The density profile corresponding to aEF (the most probable static scission point) in ^{180}Hg can be associated with a $A_H/A_L = 99/81$ mass split, which is very consistent with the observed mass asymmetry of $A_H/A_L = 100(1)/80(1)$ [8]. The minimum of the neck joining the two prefragments is located at 0.6 fm from the center of mass. Density distributions for higher-lying prescission configurations shown in Fig. 3(a) are all similar, with the heavier fragment being nearly spherical and the lighter fragment elongated. When moving closer to the $Q_{30} = 0$ line, we see that the neck is still pronounced and the fragments are elongated. That is, the symmetric configurations competing with aEF do not correspond to the two spherical ^{90}Zr nuclei. A very similar situation is obtained in HFB-SkM*, where the predicted mass split at the static scission point is $A_H/A_L = 101/79$, and in the model of Ref. [13]: $A_H/A_L \approx 103/77$.

The prescission shapes of ^{198}Hg are shown in Fig. 3(b). The mass split along aEF is 108/90 and the minimum of the neck is located at about 1.7 fm from the center of mass. Interestingly, the heavier fragment is elongated while the lighter fragment is nearly spherical, i.e., this is exactly opposite to what has been predicted for ^{180}Hg. Again, our HFB-SkM* calculations yield

a very consistent result, $A_H/A_L = 110/88$, that is close to the mass split ≈111/87 of Ref. [13].

Figure 4(a) shows the fission valley aEF for ^{180}Hg in HFB-D1S in the (Q_{20}, Q_N) plane as the scission point (small values of Q_N) is gradually approached with increasing Q_{20}. For $Q_{20} < 170$ b, the configuration sFu corresponding to two separated ^{90}Zr fragments lies above aEF [see also Fig. 1(b)]. For $Q_{20} > 170$ b an energy barrier appears between aEF and sFu. Moreover, as discussed above, a transition from aEF to sFu is going to be strongly hindered by the very different intrinsic structure of these two configurations.

We first considered the nuclei that (i) have the same N/Z ratio as the parent system; (ii) have mass numbers that reproduce the doubled mass of the outer part of the fragment situated outside the vertical line in Fig. 4(b); and (iii) have density distributions that match those of the fragments. The detailed analysis of the shape of ^{180}Hg in the near-scission configuration of aEF with $Q_{20} = 260$ b and $Q_N = 0.3$ is shown in Figs. 4(b)–4(d). Since the nuclei of ^{90}Zr and ^{72}Ge have the same N/Z ratio as that of ^{180}Hg, they are obvious candidates. The larger fragment of ^{180}Hg has a nearly spherical shape. This is consistent with the ground state of semimagic ^{90}Zr. The smaller fragment is strongly elongated. A deformed configuration of ^{72}Ge with $Q_2 = 8$ b, at an excitation energy of 3.4 MeV, fits the bill. By comparing the calculated density profiles, we see that the prescission configuration of ^{180}Hg can indeed be viewed as a molecular system consisting of spherical ^{90}Zr and deformed ^{72}Ge fragments connected by a thin neck with a slightly reduced density that contains 8 protons and 10 neutrons. At scission, the neck nucleons are shared between the two fragments. One likely split could be ^{100}Ru/^{80}Kr.

Following similar analysis for ^{198}Hg presented in Fig. 5, we conclude that its near-scission aEF configuration can be viewed as a molecular system. It consists of ^{80}Ge in its nearly spherical ground state with $Q_{20} = 2.4$ b, ^{98}Zr in a well-deformed ($Q_{20} =$ 12 b) configuration, and a neck containing 8 protons and 12 neutrons. Therefore, one likely split could be ^{108}Ru/^{90}Kr.

V. CONCLUSIONS

Our self-consistent calculations based on the nuclear DFT with SkM* and D1S effective interactions give a very consistent description of the fission process in ^{180}Hg and ^{198}Hg. By considering several collective coordinates, we were able to follow static fission and fusion pathways in the configuration space. We confirm the findings of Ref. [8], that the asymmetric fission valley aEF is well separated from fusion valleys associated with nearly spherical fragments. We conclude that the mass distribution of fission fragments in both nuclei is governed by shell structure of prescission configurations associated with molecular structures. In ^{180}Hg, both our models suggest ^{100}Ru/^{80}Kr as the most probable split—a finding that is very consistent with the experiment—and both predict symmetric elongated configurations sEF to lie rather high in energy. The most likely split predicted for ^{198}Hg is ^{108}Ru/^{90}Kr in HFB-D1S and ^{110}Ru/^{88}Kr in HFB-SkM*. Both models yield PES for this nucleus to be fairly soft in the Q_{30} direction in a prescission region, and this is expected to result in an increased yield of nearly symmetric partitions and yield a very shallow, or even two-humped, structure seen experimentally [11,12].

ACKNOWLEDGMENTS

Useful discussions with A. N. Andreyev are gratefully acknowledged. This work was supported by Grant No. DEC-2011/01/B/ST2/03667 from the National Science Centre (Poland) and the U.S. Department of Energy under Contracts No. DE-FC02-09ER41583 (UNEDF SciDAC Collaboration), No. DE-FG02-96ER40963 (University of Tennessee), No. DE-FG52-09NA29461 (the Stewardship Science Academic Alliances program), and No. DE-AC07-05ID14517 (NEUP Grant No. 00091100).

[1] H. J. Krappe and K. Pomorski, *Theory of Nuclear Fission: A Textbook*, Lecture Notes in Physics, Vol. 838 (Springer, Berlin, 2012).
[2] M. Warda, J. L. Egido, L. M. Robledo, and K. Pomorski, Phys. Rev. C **66**, 014310 (2002).
[3] H. Goutte, J. F. Berger, P. Casoli, and D. Gogny, Phys. Rev. C **71**, 024316 (2005).
[4] A. Staszczak, A. Baran, J. Dobaczewski, and W. Nazarewicz, Phys. Rev. C **80**, 014309 (2009).
[5] M. Warda, K. Pomorski, J. L. Egido, and L. M. Robledo, Int. J. Mod. Phys. E **14**, 403 (2005).
[6] W. Younes and D. Gogny, Phys. Rev. C **80**, 054313 (2009).
[7] M. Kortelainen, J. McDonnell, W. Nazarewicz, P.-G. Reinhard, J. Sarich, N. Schunck, M. V. Stoitsov, and S. M. Wild, Phys. Rev. C **85**, 024304 (2012).
[8] A. N. Andreyev *et al.*, Phys. Rev. Lett. **105**, 252502 (2010).
[9] K.-H. Schmidt *et al.*, Nucl. Phys. A **665**, 221 (2000).
[10] W. D. Myers and W. J. Swiatecki, Nucl. Phys. A **601**, 141 (1996).
[11] S. I. Mulgin, K.-H. Schmidt, A. Grewe, and S. V. Zhdanov, Nucl. Phys. A **640**, 375 (1998).
[12] M. G. Itkis *et al.*, Sov. J. Nucl. Phys. **52**, 601 (1990); **53**, 757 (1991).
[13] T. Ichikawa, A. Iwamoto, P. Möller, and A. J. Sierk (2012), arXiv:1203.2011v1 [nucl-th].
[14] P. Möller, J. Randrup, and A. J. Sierk, Phys. Rev. C **85**, 024306 (2012).
[15] A. V. Karpov, A. Kelić, and K.-H. Schmidt, J. Phys. G **35**, 035104 (2008).
[16] A. Staszczak, M. Stoitsov, A. Baran, and W. Nazarewicz, Eur. Phys. J. A **46**, 85 (2010).
[17] A. Staszczak, A. Baran, and W. Nazarewicz, Int. J. Mod. Phys. E **20**, 552 (2011).
[18] N. Schunck, J. Dobaczewski, J. McDonnell, W. Satuła, J. A. Sheikh, A. Staszczak, M. Stoitsov, and P. Toivanen, Comput. Phys. Commun. **183**, 166 (2012).
[19] J. Bartel, P. Quentin, M. Brack, C. Guet, and H.-B. Håkansson, Nucl. Phys. A **386**, 79 (1982).
[20] J. Dobaczewski, W. Nazarewicz, and M. V. Stoitsov, Eur. Phys. J. A **15**, 21 (2002).

[21] J. Dobaczewski, H. Flocard, and J. Treiner, Nucl. Phys. A **422**, 103 (1984).
[22] M. Warda and L. M. Robledo, Phys. Rev. C **84**, 044608 (2011).
[23] L. M. Robledo, HFBaxial code, (2002); J. L. Egido, L. M. Robledo, and R. R. Chasman, Phys. Lett. B **393**, 13 (1997); L. M. Robledo and G. F. Bertsch, Phys. Rev. C **84**, 014312 (2011).
[24] J. F. Berger, M. Girod, and D. Gogny, Nucl. Phys. A **428**, 23 (1984).
[25] P. Möller, D. G. Madland, A. J. Sierk, and A. Iwamoto, Nature (London) **409**, 785 (2001); N. Dubray and D. Regnier, Comput. Phys. Commun. **183**, 2035 (2012).
[26] W. Younes and D. Gogny, Phys. Rev. Lett. **107**, 132501 (2011).